J. Fluid Mech. (2006), *vol.* 551, *pp.* 175–184.
doi:10.1017/S0022112005008505 Printed in the United Kingdom

Bubble break-up in a straining flow at finite Reynolds numbers

By A. REVUELTA[1], J. RODRÍGUEZ-RODRÍGUEZ[2] AND C. MARTÍNEZ-BAZÁN[3]

[1]División de Combustión y Gasificación, CIEMAT, 28040 Madrid, Spain

[2]Departament of Mechanical and Aerospace Engineering, University of California, San Diego, La Jolla, CA 92093-0411, USA

[3]Área de Mecánica de Fluidos, Departamento de Ingeniería Mecánica y Minera, Universidad de Jaén, Campus de las Lagunillas, 23071 Jaén, Spain

(Received 11 October 2005 and in revised form 9 December 2005)

It has recently been shown that the behaviour of a gas bubble in a uniaxial straining flow can be used as a simplified model to describe some important aspects of the more complex, turbulent bubble break-up problem, provided that the Reynolds and the Weber numbers are sufficiently large. In the present investigation, we extend that work and, using a level-set numerical scheme, we analyse the influence of the bubble Reynolds number on break-up time, t_b, for supercritical Weber numbers, $We > We_c$, where We_c is the critical Weber number. It is observed that the viscosity introduces corrections of $O(1/Re)$ in the break-up time obtained in the limit $Re \to \infty$. In addition, the action of other possible mechanisms of break-up at subcritical Weber numbers, $We < We_c$, is also explored.

1. Introduction

The transport of gas bubbles immersed in a turbulent immiscible flow is commonly observed in engineering and nature. The break-up of bubbles and their interaction with the surrounding flow are responsible for the size distribution generated. This phenomenon plays a role in many physico-chemical processes such as multiphase chemical reactions, gas absorption, phase change or extinction techniques using sprays in reactive atmospheres. The deformation and break-up of bubbles determine the interface area between the two phases and, therefore, the rate of transfer of heat, mass and momentum. Thus, theoretical models for bubble size distributions in blenders, mixers and any two-phase flows require *a priori* predictions of a break-up criterion (Lasheras *et al.* 2002).

Kolmogorov (1949) was the first to investigate the drop break-up (dispersed phase) into a turbulent, homogeneous and isotropic flow (continuous phase) of the same density. Hinze (1955) reviewed the available experimental data on the turbulent break-up of particles and concluded that, despite the complexity of the problem, the different morphologies observed could be classified into three kinds, i.e. lenticular, cigar-shape and bulgy. He also stated that, to understand the particle deformation problem, it was not necessary to consider the entire turbulent field but only the flow pattern observed in the region near the particle. Therefore, he classified such local patterns into six different types (see figures 1 and 2 of Hinze 1955). According to the Kolmogorov–Hinze theory, the turbulent break-up of a particle is determined by the competing effects of the pressure fluctuations acting on its surface and the restoring forces due to surface tension. The ratio of the two forces gives the so-called turbulent Weber

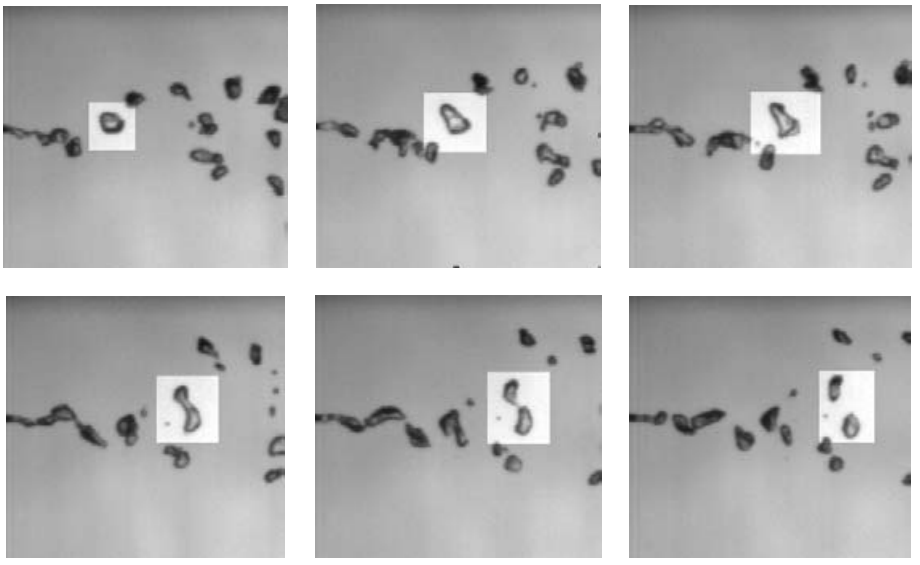

FIGURE 1. High-speed video images, recorded at 1000 f.p.s., of the break-up of an air bubble (highlighted) immersed in a turbulent water jet. The radius of the bubble is $a_0 \approx 2.12\,\mathrm{mm}$ which, for the experimental flow conditions, corresponds to a bubble Reynolds number of $Re \approx 1360$ and a Weber number of $We \approx 12$.

number, *We*. Recently, Risso & Fabre (1998) extended the classical Kolmogorov–Hinze theory, identifying two possible break-up mechanisms. The first corresponds to the above mentioned balance of forces, but the second is simply a resonance mechanism that takes into account the interaction of a bubble with several consecutive turbulent structures. Therefore, if the turbulence is moderate, an individual eddy would not break an initially spherical bubble. However, a sequence of vortices could deform it progressively and eventually break it up.

If the main physical aspects of the process are properly retained, the use of simplified models can help to understand the break-up phenomenon, without performing highly expensive three-dimensional simulations. Images of the bubble morphology during the break-up process, similar to those shown in figure 1, indicate that an initially round bubble is stretched along a preferential direction until it breaks. Consequently, the type of break-up identified in our experimental observations corresponds to the classical cigar-shape breakage proposed by Hinze (1955) and, thus, as in Rodríguez-Rodríguez, Gordillo & Martínez-Bazán (2006), the process can be considered approximately axisymmetric.

The fundamental characteristics of the turbulent break-up of bubbles and drops has been described by various authors with different approximations. In particular, note the meticulous investigations of Kang & Leal (1987); Kang & Leal (1989, 1990), who characterized the deformation of a bubble immersed in an axisymmetric, uni-axial and bi-axial straining flow at both finite and infinite Reynolds numbers. In a sense we extend their work by providing further information about the dependence of the break-up time on the parameters of the problem. In addition, in our simulations, we allow the bubble to move along the axis of symmetry with the aim of studying the effect of the finite residence time on the break-up process.

2. Problem formulation and numerical method

The velocity field far away from the bubble was assumed to be the steady, axisymmetric and hyperbolic flow sketched in figure 2, and given by the following

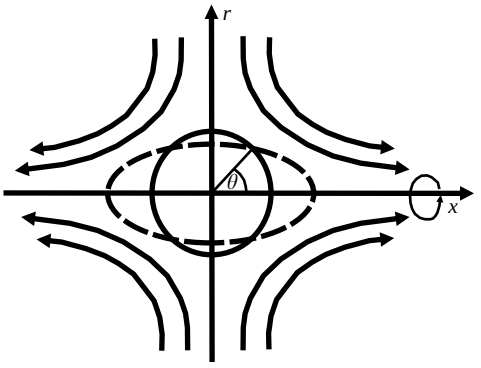

FIGURE 2. Sketch of the flow field considered.

dimensional velocity potential:

$$\tilde{\Phi} = \frac{M}{a_0}(-\tilde{r}^2 + 2\tilde{x}^2), \tag{2.1}$$

where M is the flow strength and a_0 is the radius of the bubble. Scaling the lengths, times and velocities with a_0, $a_0/8M$ and $8M$ respectively, the dimensionless boundary condition at $(r, x) \to \infty$ can be expressed as

$$\Phi \to -r^2/8 + x^2/4, \quad u = x/2 \qquad v = -r/4. \tag{2.2}$$

Here x and r are the axial and radial coordinates and u and v are the axial and radial velocities, respectively. Using the density, ρ_w, and the viscosity, μ_w, of the continuous, liquid phase to make dimensionless the incompressible Navier–Stokes equations, one obtains

$$\nabla \cdot \boldsymbol{u} = 0, \tag{2.3}$$

$$\boldsymbol{u}_t + (\boldsymbol{u}\cdot\nabla)\boldsymbol{u} = \frac{1}{\rho(\phi)}\left[-\nabla p + \frac{1}{Re}\nabla\cdot[\mu(\phi)\nabla\boldsymbol{u} + \mu(\phi)\nabla\boldsymbol{u}^T] - \frac{1}{We}\kappa(\phi)\,\delta_\epsilon(\phi)\nabla\phi\right], \tag{2.4}$$

where $Re = \rho_w\,(8M)\,a_0/\mu_w$ and $We = \rho_w\,(8M)^2\,a_0/\sigma$ are the characteristic Reynolds and Weber numbers respectively. The Navier–Stokes equations were solved with a projection method where $\rho(\phi) = \rho_a + (1-\rho_a)\,H_\epsilon(\phi)$ and $\mu(\phi) = \mu_a + (1-\mu_a)\,H_\epsilon(\phi)$ are the local values of the density and viscosity at any given position, ϕ, from the interface. Here $\kappa(\phi) = \nabla\cdot\boldsymbol{n} = \nabla\cdot(\nabla\phi/|\nabla\phi|)$ is the local curvature, ρ_a and μ_a are the dimensionless density and viscosity of the gas phase, and ϕ represents the level-set function, whose time evolution can be given by the following advection equation:

$$\phi_t + \boldsymbol{u}\cdot\nabla\phi = 0, \tag{2.5}$$

with $\phi(t) = 0$ indicating the position of the interface at any given time t. $H_\epsilon(\phi)$ and $\delta_\epsilon(\phi)$ are the Heaviside and Dirac functions, adequately regularized as

$$H_\epsilon(\phi) = \begin{cases} 0 & \text{if } \phi < -\epsilon \\ 1/2\ [1 + \phi/\epsilon + 1/\pi\, sin(\pi\phi/\epsilon)] & \text{if } |\phi| \leqslant \epsilon \\ 1 & \text{if } \phi > \epsilon, \end{cases} \tag{2.6}$$

$$\delta_\epsilon(\phi) = \begin{cases} 0 & \text{if } |\phi| > \epsilon \\ 1/2\ [1/\epsilon + 1/\epsilon\, cos(\pi\phi/\epsilon)] & \text{if } |\phi| \leqslant \epsilon, \end{cases} \tag{2.7}$$

where ϵ is a numerical parameter that represents the thickness of the interface. The Navier–Stokes equations (2.3) and (2.4) were integrated in a staggered grid, using a semi-implicit temporal Crank–Nicholson scheme for the viscous terms, and an explicit

Adams–Bashforth scheme for the convective terms, which were spatially discretized with a third-order ENO scheme. The level-set equation (2.5) was integrated with a semi-implicit, second-order advection operator partition. The initial condition used for the simulations corresponded to a flow field initially at rest, with a spherical bubble located at the stagnation point of the imposed hyperbolic field, as sketched in figure 2.

2.1. *Re-distance algorithm*

When the level-set equation is solved, the value of ϕ can be distorted by the flow field and the numerical diffusion of the numerical method. This problem can be avoided by defining a new distance function, d, every time step and solving the so-called re-distance equation to satisfy the condition $|\nabla\phi| = 1$ near the interface (Sussman *et al.* 1998),

$$d_\tau = \frac{\partial d}{\partial \tau} = \mathrm{sign}(\phi)(1 - |\nabla d|) + \lambda\, H'_\epsilon(\phi)|\nabla\phi|. \tag{2.8}$$

Equation (2.8), where λ is a constant to be evaluated at each computational cell as

$$\lambda_{ij} = -\frac{\displaystyle\int_{\Omega_{ij}} H'_\epsilon(\phi)\,\mathrm{sign}(\phi)(1 - |\nabla d|)\,\mathrm{d}\Omega_{ij}}{\displaystyle\int_{\Omega_{ij}} H'^2_\epsilon(\phi)|\nabla\phi|\,\mathrm{d}\Omega_{ij}}, \tag{2.9}$$

must be solved with the initial condition $d(\boldsymbol{x}, \tau = 0) = \phi(\boldsymbol{x}, t)$. This Hamilton–Jacobi equation, with the additional constraint $\lambda\, H'_\epsilon(\phi)|\nabla\phi|$, which corresponds to the re-distance step, was solved with a third-order TVD Runge–Kutta temporal scheme. Similarly, a third-order ENO scheme was used for the spatial discretization.

The level-set code was adequately validated by solving the two-phase flow problems proposed in the seminal investigation of Sussman & Smereka (1997), i.e the vibration modes of the bubble and the rise velocities of a bubble for different conditions. In addition, to make sure that the method was able to accurately determine the proper values of the critical Weber number and the break-up times, the results obtained for $Re \gg 1$ were successfully compared with those given by Rodríguez-Rodríguez *et al.* (2006) using a boundary element method code in the limit $Re \to \infty$. The simulations presented here were performed in a $(r, x) = [0, 3] \times [-6, 6]$ domain with $\mathrm{NR} \times \mathrm{NX} = 66 \times 256$ grid points. Furthermore, in most of the cases reported, mass was conserved within a 99 % of accuracy, being 97 % in the most critical cases, i.e. high Reynolds numbers and low Weber numbers. We also carried sensitivity analyses of the results to grid refinement and domain size using a larger domain, $(r, x) = [0, 6] \times [-9, 9]$, and a finer grid, $\mathrm{NR} \times \mathrm{NX} = 132 \times 396$, in some representative cases, without observing significant differences.

3. Results and discussion

The results presented in this section were obtained for the values of $\rho_a = 0.001$ and $\mu_a = 0.01$ which approximately correspond to the air-to-water density and viscosity ratios. In accordance with the results of Kang & Leal (1987); Kang & Leal (1989), our simulations show two possible scenarios depending on the value of the Weber number. For We larger than a critical value, We_c, the bubble breaks into two bubbles after a certain time. However, the formation of small satellites was also observed at Weber numbers slightly larger than the critical one (see figure 3), and at the lower range of Reynolds numbers calculated. On the other hand, if $We < We_c$, the bubbles oscillate with an increasing frequency and a decreasing amplitude as We decreases. Figure 4 shows the time evolution of the bubble deformation, D, defined as the distance between

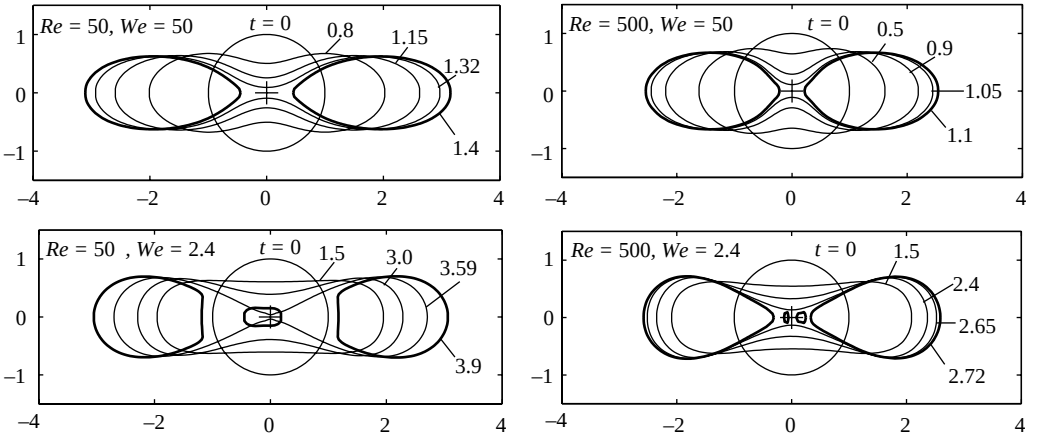

FIGURE 3. Bubble break-up patterns for $We = 50$, 2.4 and $Re = 50$, 500.

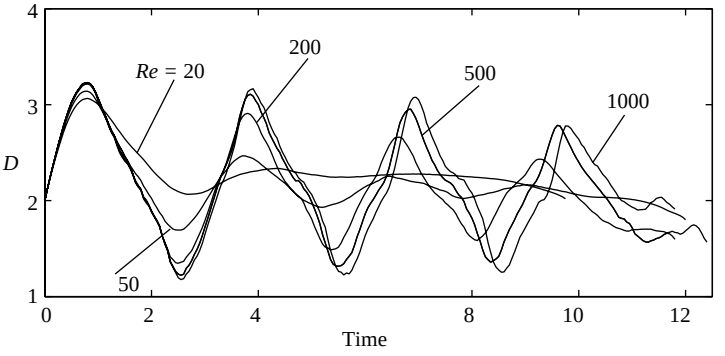

FIGURE 4. Temporal oscillations of the bubble deformation along the x-axis, D, for a sub-critical Weber number, $We = 1.5$, and different Reynolds numbers.

the edges of the bubble along the x-axis, for $We = 1.5$ and different Reynolds numbers. It can be observed that the damping of the oscillations is a decreasing function of Re. Thus, the bubbles break if the inertia of the outer fluid is sufficiently large to overcome the confining effects of surface tension or, similarly, if $We > We_c$. However, for subcritical Weber numbers, $We < We_c$, the bubble could still break due to a previous deformation or the fluctuating strength of the outer flow field.

3.1. *Dependence of the critical Weber number, We_c, on the Reynolds number, Re*

Unfortunately, there are no detailed experimental results of the dependence of We_c on Re to compare with. However, comparing our results with those reported by Kang & Leal (1987) we observed some appreciable differences. We found that We_c does not vary with Re at high Reynolds numbers ($We_c = 2.22 \pm 0.005$ for $Re \geqslant 20$), and that the value of We_c tends to zero in the limit $Re \to 0$ for $Re \sim 1$ (for example, $We_c(Re) = 0.5(1), 1.6(5)$). On the other hand, according to our definition of the Weber number, the values reported by Kang & Leal (1987) are $We_c(Re) = 1.8(10), 4.2(100), 5.4(\infty)$. The discrepancies in the We_c, found at high Reynolds numbers, are a consequence of the different initial conditions used in the two studies, and the different criteria to determine We_c. While in Kang & Leal the critical Weber number is given by the maximum value of We for which there exists a steady solution for the shape of the bubble, in the present work it is defined as the minimum value of We required

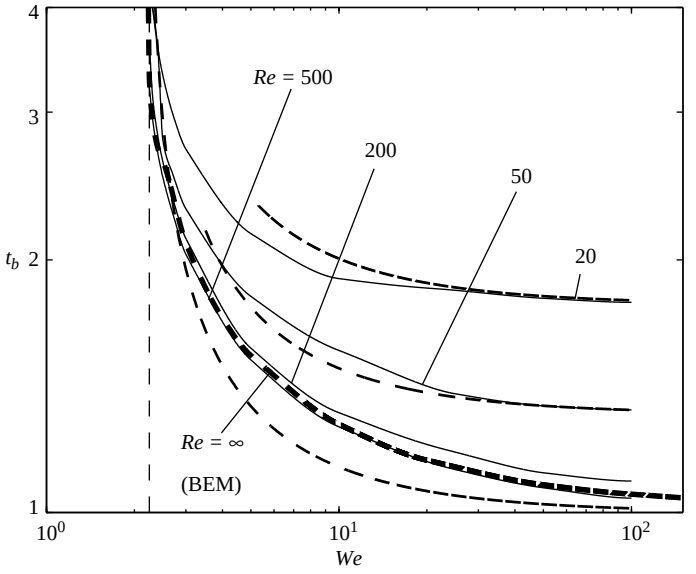

FIGURE 5. Dependence of the break-up time, t_b, on the Weber number for different Reynolds numbers. Dashed lines correspond to the approximated relation $(1+15.5/Re)(1-We_c/We)^{-1/2}$ given by (3.1). The figure also shows that the results obtained with the level-set method at $Re \gg 1$ agree with those given by a boundary-element method in the limit $Re \to \infty$.

to break a spherical bubble initially at rest. It is important to note that we may observe break-up events at values of *We* for which Kang & Leal reported steady solutions, especially at high *Re*, since in our simulations the initial deformation of the bubble may be sufficiently far from the non-spherical, equilibrium shape, a fact already pointed out by Kang & Leal (1987).

3.2. *Dependence of break-up time on the Weber and Reynolds numbers*

Figure 5 shows the dependence of the break-up time, t_b, of a bubble on *Re* and *We* for supercritical Weber numbers. In this figure we have also plotted the results obtained with a boundary element method, BEM, in the limit $Re \to \infty$ to demonstrate that the level-set method employed in this work reproduces the same results at $Re \gg 1$. It can be observed that t_b increases as the Weber number and the Reynolds number decrease. However, although the numerical method may not properly describe the final stages of the process, it does not affect to the break-up time obtained since the final collapse of the neck of the bubble occurs at times very short compared with t_b; see Gordillo *et al.* (2005).

Considering an appropriate definition for the Weber number, Martínez-Bazán, Montañes & Lasheras (1999) proposed a model for the turbulent break-up time of bubbles, applicable in the limit $Re \to \infty$, given by $t_b^{\infty} \approx (1 - We_c/We)^{-1/2}$ or, similarly, $g^* = 1/\beta(1 - We_c/We)^{1/2}$ with g^* being the dimensionless break-up frequency. Rodríguez-Rodríguez *et al.* (2006) showed that, in the limit $Re \to \infty$, this expression for g^* accurately predicts the experimentally measured break-up time of bubbles in turbulent flows once the constant $\beta = \beta(\infty)$ is correctly chosen. Furthermore, our numerical simulations showed that the effect of viscosity introduces corrections of the break-up time of $O(Re^{-1})$ (see figure 5), indicating that the break-up time should, indeed, behave as

$$t_b \approx (1 + C\,Re^{-1})(1 - We_c/We)^{-1/2}. \tag{3.1}$$

Thus, to account for the viscous effects, we can extend the above break-up model suggesting a dependence of β on Re as $\beta(Re) = \beta(\infty)(1 + C/Re)$. On the other hand, following the ideas of Martínez-Bazán *et al.* (1999), and including the viscous stresses acting the surface of the bubble, of $O(\mu_w \Delta u/a_0)$, in their equation (4.7), the bubble break-up time can be estimated as

$$\bar{t}_b \approx \frac{a_0}{\bar{u}_b} = \frac{a_0}{\sqrt{(\Delta u)^2 - C_1\,\mu_w\,\Delta u/(\rho_w\,a_0) - C_2\,\sigma/(\rho_w\,a_0)}}, \tag{3.2}$$

where $\Delta u = \sqrt{\overline{|\boldsymbol{u}(\boldsymbol{x} + a_0, t) - \boldsymbol{u}(\boldsymbol{x}, t)|^2}}$ is the root-mean-squared velocity difference between two points separated a distance a_0. Expressing equation (3.2) in dimensionless form gives

$$t_b \approx \frac{1}{\sqrt{1 - C_3/Re - We_c/We}}, \tag{3.3}$$

which represents a correction to the break-up time model developed by Martínez-Bazán *et al.* (1999) for $Re \to \infty$. Note that the break-up time given by equation (3.1) can also be obtained from (3.3) in the double limit of $Re \gg 1$ and $We \gg 1$.

Although the lenticular break-up pattern was not identified in our experimental observations, we also explored the possible break-up of a bubble subjected to a bi-axial straining flow by changing the sign of M in equation (2.1). Our results indicated that the bubble initially deforms, forming a torus that may eventually break at times much larger than those obtained in a uni-axial flow. Thus, we consider that, in real turbulent flows, the break-up of bubbles is mainly caused by their interaction with turbulent structures that generate a uni-axial straining flow around the bubble.

3.3. *Resonance break-up at subcritical Weber numbers, $We < We_c$*

As suggested by Kang & Leal (1990), we explored the possibility of finding break-up events at sub-critical Weber numbers, $We < We_c$, caused by a resonance mechanism between the oscillation of the bubble immersed in the hyperbolic axisymmetric flow and the fluctuations of the flow strength, $M(t) = M_0(1 - \delta \cos \omega t)$, where ω was selected to be the frequency of oscillation of a spherical bubble in the corresponding stationary straining flow of strength M_0, and δ is the amplitude of the fluctuations. A multiple-scale analysis of the dynamical system of Kang & Leal (1990) shows that small oscillations of the flow strength produce bubble deformations of higher order of magnitude, $O(\delta^{1/3})$, for long dimensionless times of $O(\delta^{-2/3})$, due to resonance. Such deformations may eventually break the bubble if they are sufficiently large. Therefore, we pursued a numerical study of the effect of an oscillating flow field on bubble break-up, and its dependence on the Reynolds number. Figure 6(*a*) shows the temporal evolution of bubble deformation, D, along the x-axis for different values of the oscillation amplitude, δ, at $Re = 500$, $We = 1.5$ and $\omega = 2$. The amplitude of D is seen to increase with δ, leading to bubble break-up for $\delta = 0.25$ in this case. It is important to indicate that the residence time of the bubble in the hyperbolic flow decreases as δ increases, making the resonance mechanism less effective than the predictions of Kang & Leal (1990). Consequently, the amplitude of the oscillation required to break the bubble is larger than initially expected. As illustrative example, figure 6(*b*) shows the dependence of the minimum value of the oscillation amplitude needed to break the bubble, δ_b, on Re for $We = 1.5$ and $\omega = 2$. The value of δ_b is seen to increase as Re decreases due to the attenuating effect of viscosity. Similarly, the value of δ_b also diminishes as the Weber number increases towards the critical value.

3.4. *Other mechanisms of bubble break-up at subcritical Weber numbers*

In addition to the above described bubble break-up mechanisms, we also investigated other possible scenarios, namely the volume (density) fluctuations of the bubble

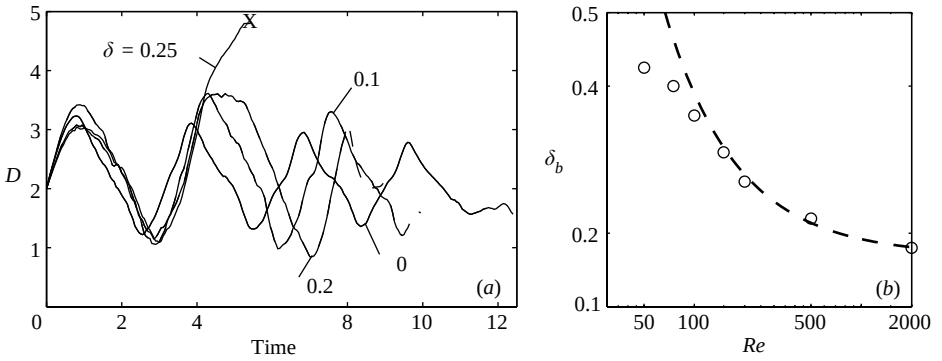

FIGURE 6. (*a*) Temporal oscillations of D for $Re = 500$, and $We = 1.5 < We_c$ and $\omega = 2$ for different values of δ. (*b*) Maximum fluctuation leading to bubble break-up as function of the Reynolds number. Dashed line indicates the approximate relation $0.17 + 22/Re$.

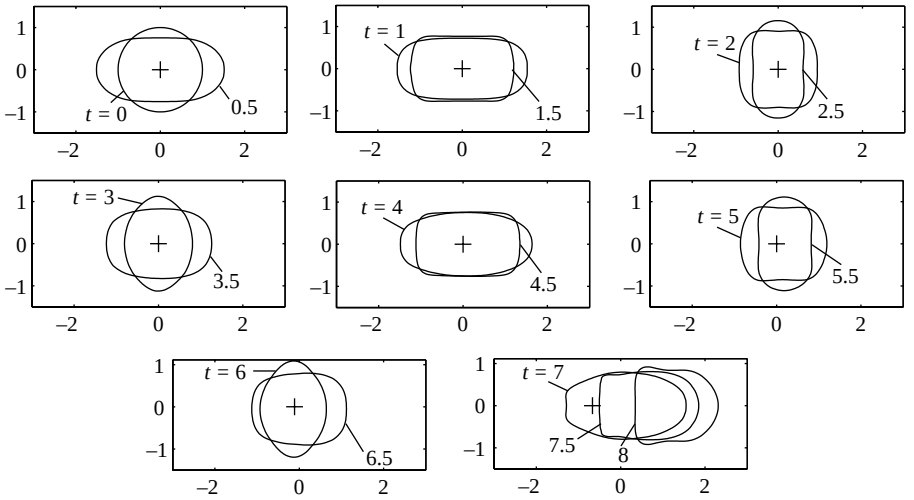

FIGURE 7. Temporal evolution of a bubble in a uniaxial straining flow for $We = 1.5$ and $Re = 1000$.

and the chaotic oscillations of the interface at frequencies lower than the resonance one caused by the periodic fluctuations of the flow field strength, a mechanism postulated by the dynamic model of Kang & Leal (1990).

The possible break-up by chaotic interface oscillations was never observed in our simulations since the bubble always escaped from the stagnation point, at times $t \sim O(10)$, before breaking up. A characteristic example is shown in figure 7. Note that the numerical simulations agree with the experimental evidence presented in figure 8 that show that, although the highlighted bubble is initially trapped and stretched by a local straining structure, it escapes from the flow without breaking up. This was never observed by Kang & Leal in their simulations because their method anchored the bubble at the centre of the flow field, without letting it move freely within it.

The investigations of Kang & Leal mentioned above, predate the recent interest in the coupling between the shape and the volume oscillations of the bubble (Yang, Feng & Leal 1993) and, therefore, they assumed bubbles of constant volume or, similarly, constant gas density. Furthermore, in a recent review (Feng & Leal 1997), the results provided by Kang & Leal were considered limited, and not applicable

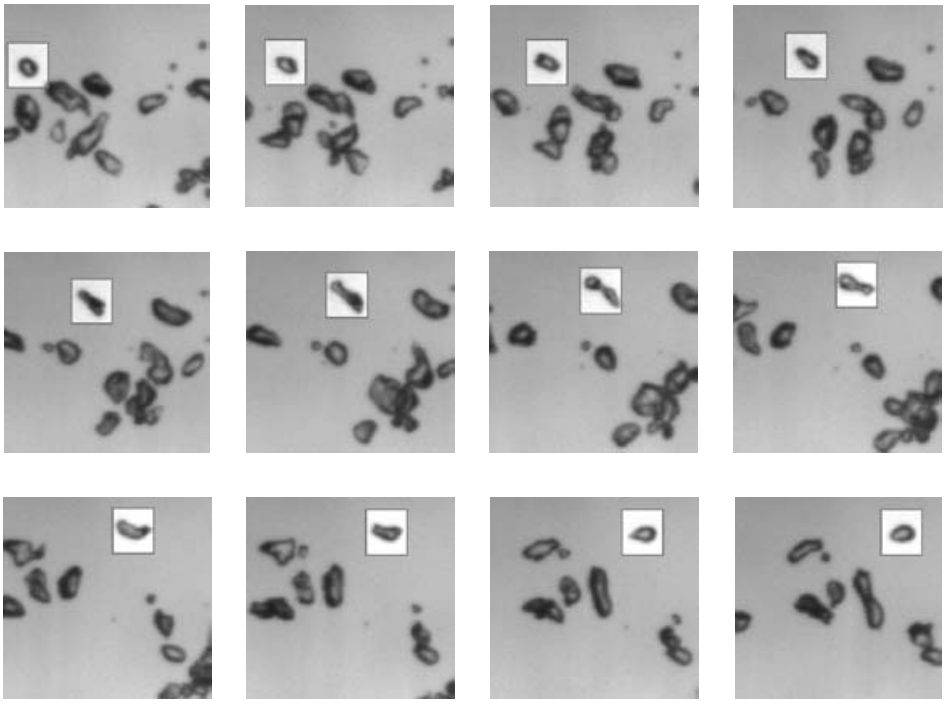

FIGURE 8. High-speed video images of an air bubble (highlighted) escaping from the local hyperbolic flow.

to all kinds of flow. Although the experiments reported here do not show large variations of volume, we tried to roughly evaluate the relevance of the bubble volume (density) fluctuations on the deformation and subsequent break-up due to a resonance mechanism at sub-critical Weber numbers. Thus, we adapted the initially incompressible level-set code to include temporal bubble density variations of the type $\rho(t) = \rho_o[1 - \delta_\rho \cos(\omega_\rho t)]$. The advection equation that describes the evolution of the interface was modified, including an additional radial expansion velocity to be determined from the bubble volume variation at any time. The simulations did not indicate the existence of any shape–volume coupling (resonance) effect, at least during the finite residence time of the bubble within the hyperbolic flow. Of course, the coupling mechanism of shape and volume oscillations is too complex to be described accurately by such simple model, and one would expect a feedback mechanism to the volume oscillations from the shape ones. However we can conclude that the compressibility effects are negligible in the bubble break-up phenomenon described here, since the short residence time of the bubble within the flow field does not permit an effective interaction between the shape and volume fluctuations.

4. Conclusions

In this investigation we have extended the work by Rodríguez-Rodríguez *et al.* (2006), performed in the limit $Re \to \infty$, to finite Reynolds numbers. The application of the level-set method to the simplified model allows us to explain some of the fundamental aspects of bubble break-up, including the computation of the break-up time and its dependence on Re, as well as the analysis of possible break-up mechanisms taking place at subcritical Weber numbers. Numerical simulations performed for a wide range of We and Re indicate that the break-up time follows reasonably well the equation $t_b \approx (1 + C\,Re^{-1})(1 - We_c/We)^{-1/2}$ for sufficiently large Weber numbers,

$We > 20$, introducing a correction of $O(Re^{-1})$ due to viscous effects at high Weber numbers. In addition, a weak dependence of the critical Weber number, We_c, on the Reynolds number is shown for $Re \gg 1$.

Regarding the possible break-up mechanisms at subcritical Weber numbers, we have also observed break-up events due to resonance between the natural oscillations of the bubble and the fluctuations of the flow strength, $M(t)$. The amplitude of the flow-field fluctuations leading to break-up depends on the Reynolds number as $\delta_b = \delta_b^{\infty} + O(Re^{-1})$. However, no break-up phenomenon caused by other possible mechanisms was detected, i.e. the chaotic shape oscillations of the interface or shape–volume resonance with a variable bubble density, since the residence time, $O(10)$, of the bubble in the hyperbolic flow was always shorter than the time required to break it up. This result may be in agreement with experimental observations in real flows, where the turbulent structure causing the uniaxial straining around the bubble weakens and vanishes at times of the order of the convective time.

The authors wish to thank Dr Gordillo for providing the results calculated with a boundary element method to validate our level-set code. This collaborative research was supported by the Spanish MCyT under Projects# DPI2002-04550-C07 and DPI2005-08654-01. A.R. also acknowledges the support of the Ramón y Cajal program.

REFERENCES

Feng, Z. C. & Leal, L. G. 1997 Nonlinear bubble dynamics. *Annu. Rev. Fluid Mech.* **29**, 201–243.

Gordillo, J. M., Sevilla, A., Rodríguez-Rodríguez, J. & Martínez-Bazán, C. 2005 Axisymmetric bubble pinch-off at high Reynolds numbers. *Phys. Rev. Lett.* **95**, 194501.

Hinze, J. O. 1955 Fundamentals of the hydrodynamics mechanism of splitting in dispersion processes. *AIChE J.* **1**, 289–295.

Kang, I. S. & Leal, L. G. 1987 Numerical solution of axisymmetric, unsteady free-boundary problems at finite Reynolds number. I. Finite-difference scheme and its application to the deformation of a bubble in a uniaxial straining flow. *Phys. Fluid.* **30**, 1929–1940.

Kang, I. S. & Leal, L. G. 1989 Numerical solution of axisymmetric, unsteady free-boundary problems at finite Reynolds number. II. Deformation of a bubble in a biaxial straining flow. *Phys. Fluids* A **1**, 644–660.

Kang, I. S. & Leal, L. G. 1990 Bubble dynamics in time-periodic straining flows. *J. Fluid Mech.* **218**, 41–69.

Kolmogorov, A. N. 1949 On the breakage of drops in a turbulent flow. *Dokl. Akad. Navk. SSSR* **66**, 825–828.

Lasheras, J. C., Eastwood, C., Martínez-Bazán, C. & Montañes, J. L. 2002 A review of statistical models for the break-up of an immiscible fluid immersed into a fully developed turbulent flow. *Intl J. Multiphase Flow* **28**, 247–278.

Martínez-Bazán, C., Montañes, J. L. & Lasheras, J. C. 1999 On the break-up of an air bubble injected into a fully developed turbulent flow. Part 1. Break-up frequency. *J. Fluid Mech.* **401**, 157–182.

Rodríguez-Rodríguez, J., Gordillo, J. M. & Martínez-Bazán, C. 2006 Break-up time and morphology of drops and bubbles in a high Reynolds number flow. *J. Fluid Mech.* **548**, 69–86.

Risso, F. & Fabre, J. 1998 Oscillations and breakup of a bubble immersed in a turbulent field. *J. Fluid Mech.* **372**, 323–355.

Sreenivasan, K. R. 1995 On the universality of the kolmogorov constant. *Phys. Fluids.* **11**, 2778–2784.

Sussman, M., Fatemi, E., Smereka, P. & Osher, S. 1998 An improved level-set method for incompressible two-phase flows. *Computers Fluids* **27**, 663–680.

Sussman, M. & Smereka, P. 1997 Axisymmetric free boundary problems. *J. Fluid Mech.* **341**, 269–294.

Yang, S. M., Feng, Z. C. & Leal, L. G. 1993 Nonlinear effects in dynamics of shape and volume oscillation for a gas bubble in an external flow. *J. Fluid Mech.* **247**, 417–454.